LAT Aerospace

Team 99

Executive Summary

Our task is to design a high-lift wing and propulsion mechanism configuration for an STOL aircraft. For proceeding towards this problem statement, we begin by mathematically modelling the core components of an aircraft - namely the Thrust Plant (or the Propulsion system) and the Wing. As we refine our mathematical concept, we continuously and iteratively verify our results using Computational Fluid Dynamics Techniques.

Our preliminary research lead us to a hypothesis, that for an STOL aircraft of the scale required by LAT Aerospace, a Distributed Electric Propulsion (DEP) system, composed of Propellers driven by Electric Motors is probably the most optimal thrust device. This mechanism alone has little effect on the lift targets desired, and thus needs to be coupled with optimally designed wings and control surfaces.

Standard rectangular wings cannot provide enough lift to take off at such low speeds as desired, thus exotic mechanisms are integrated to acheive desired performance indices. Blown Flaps, Upper Surface Blown Wings, etc. are some extensively researched topics that can enhance the lift capability of aircrafts. Our research finds Blown Flaps to be optimal, because of the mechanical simplicity, and higher efficiencies than other mechanisms.

In our research we focused on accurately refining our mathematical formulation for the above devices, and an attempt to parameterize the equations, in order to allow us to use constraint optimization techniques to get optimal configurations of the aforementioned components.

In this paper, we were able to mathematically model the propellers and the blown wings to a reasonable level of accuracy, with sufficient parameterization which will help us move forward in little time. This has given us a firm position towards proceeding with an in depth research for reaching the ultimate solution.

In further stages we will be working on the optimization techniques and detailed study about various other factors of an aircraft that are influenced by the design decisions made in relevance to the posed problem, and how the practical implementation of these decisions can be carried out by the team at LAT Aerospace.

Contents

1 Thrust Plant **1**
- 1.1 Introduction . . . 1
- 1.2 Propeller . . . 2
  - 1.2.1 Mathematical Model . . . 2
    - 1.2.1.1 Momentum Theory . . . 3
    - 1.2.1.2 Blade Element Momentum theory . . . 5
  - 1.2.2 Validation using Computational Fluid Dynamics . . . 7
    - 1.2.2.1 Introduction to the Virtual Blade Model . . . 7
    - 1.2.2.2 Model Assumptions . . . 8
    - 1.2.2.3 Advantages of using the model . . . 8
    - 1.2.2.4 CFD Setup for Propeller Simulation . . . 9
    - 1.2.2.5 Airfoil File Format . . . 10
    - 1.2.2.6 Solver setup . . . 11
    - 1.2.2.7 VBM Field variables . . . 14
    - 1.2.2.8 VBM Output and Post-processing . . . 15
- 1.3 EDF . . . 17

2 Wing **18**
- 2.1 Introduction . . . 18
- 2.2 Wing Without Flaps . . . 18
  - 2.2.1 Overview . . . 18
  - 2.2.2 Mathematical Model . . . 18
  - 2.2.3 Bringing in the Third Dimension . . . 21
    - 2.2.3.1 Introduction . . . 21
    - 2.2.3.2 OpenVSP and VSPAero . . . 21
    - 2.2.3.3 Geometry Setup in OpenVSP . . . 21
    - 2.2.3.4 VSPAero . . . 22
    - 2.2.3.5 Results Manager . . . 22
    - 2.2.3.6 Python API . . . 22
  - 2.2.4 Validation using Computational Fluid Dynamics . . . 22
    - 2.2.4.1 Geometry Construction . . . 23
    - 2.2.4.2 Meshing . . . 24
    - 2.2.4.3 Y+ Calculation . . . 24
    - 2.2.4.4 Setup . . . 25
    - 2.2.4.5 Results and Discussion . . . 26

2.2.5 A Comparitive Study 28
2.3 Wing With Flaps 29
2.3.1 Overview 29
2.3.2 Mathematical Model 29
2.3.3 Bringing in the Third Dimension 30
2.3.4 Analysis using Computational Fluid Dynamics 30
2.4 Blown Wing With Flaps 31
2.4.1 Overview 31
2.4.2 Mathematical Model 31
2.4.2.1 Model Validation and Error Analysis 34
2.4.2.2 Future Advancements 35
2.4.3 CFD 35

3 Planned Timeline **36**

Bibliography **37**

Chapter 1

Thrust Plant

1.1 Introduction

One of the first components of an aircraft we need to start working on is the Thrust Plant, which may also be called the Propulsion System. These systems provide the thrust to move the aircraft along the runway to build up speed, which is leveraged by the wings to provide the necessary lift for the aircraft to take off and stay in the air.

Thrust plants can broadly be classified into two categories, Non-Air Breathing Systems (like Rocket Engines, Ionic Propulsion, etc.) or Air Breathing Systems. The Air Breathing Systems in themselves can be classified into families based on what kind of technology runs them, like Gas-Turbine / Jet Engines (Turbofan, Turbojet, Turboprop, Ramjet, Scramjet, etc.) or Propulsive Disk Systems (Rotor-based, Propeller, Ducted Fan, etc.).

Thrust plants like Rocket Engines are not designed for atmospheric cruise flight and are highly inefficient for short-range transport as is desired. Others like Ionic Propulsion provide an extremely low Thrust-to-Weight ratios, which make them impractical for an aircraft. Within Air Breathing systems, Engines based on Gas-Turbines or Jet Engines are unsuitable for urban operations due to their extremely low efficiency in low-speed low-altitude conditions which we are targeting. Moreover, their high exhaust velocities result in excessive noise, heat and downwash, making them unfavorable for flight around residential and other urban regions.

This leaves the Propulsive Disk Systems, which generate thrust by imparting momentum to a large mass of air. These systems - comprising of Rotors, Propellers, and Electric Ducted Fans (EDFs) - are more efficient at low-speed flights. Other capabilities like electric drive integration make them ideal candidates for Distributed Electric Propulsion (DEP) architectures which are commonly used in other STOL aircrafts targeting a similar audience, like the ones made by Electra[1].

In this Chapter we have covered Propellers and EDFs, and done a comparative study over why one must perform better than the other in our desired application. Rotor-based configurations were excluded from this analysis, as their design characteristics are more similar to vertical or hover-capable systems instead of fixed-wing aircrafts.

1.2 Propeller

The propulsion system is crucial to obtain very high and efficient lift. Three major types of propulsion systems were suggested to work upon that are Open Propellers, EDFs, and Rotors. For the initial analysis we have ruled out rotors (variable pitch) and focused on the first two to obtain required thrust with minimum power.

To predict the performance of any propeller mathematically is difficult considering the airflow complexity that exists in a flight during take-off or Landing so we consider the propeller to be stationary and fixed in space. The major factors that affect the thrust it generates are: The blade geometry, Rpm, Relative velocity of wind and Airfoil used in the blade. The governing theorems and equations to solve all these factors are given by Navier Stokes Equations which are non-linear PDEs and difficult to solve. They can be simplified by various assumptions like inviscid, incompressible and steady flow but still they remain difficult to solve in 3 dimensions so we need to look into other theories to derive a mathematical model that can accurately predict a Propeller's performance. For this purpose we have considered Blade Element Momentum Theory which comprises of BET – Blade Element Theory and Momentum Theory that are used together.

The BET considers each blade section as a 2D airfoil to produce aerodynamic forces and by integrating these sectional loads over the length of the blade and averaging the result over a rotor revolution.

Momentum theory on the other hand deals with the propeller as a thin disk with some velocity and pressure distribution on its faces and at infinity. It basically comprises of conservation laws and deals with the work done on the fluid by the propeller.

Combining these theories we can make a mathematical model that includes all the factors which are not considered in any one of them.

1.2.1 Mathematical Model

The methods are derived from [2]Let us assume a propeller of an aircraft which is cruising at some altitude in forward flight, it would feel a relative wind velocity axially, say at V m/s, that is just the forward speed of the aircraft and the propeller is rotating at an angular speed, say,

$$\Omega$$

rad/s. Then the realtive velocity of the blade tip with respect to the wind will be

$$V_R = \sqrt{V^2 + (\Omega r)^2}$$

This is based on the assumption that the airfoil of blade has no effect on the wind velocity, which is not correct. As like any other airfoil, this will also generate some lift and drag force on the blade element which will affect the relative wind velocity. We account for this as axial and azimuthal induction factors say a and b, respectively, such that

$$V_R = \sqrt{(1+a)^2V^2 + (1-b)^2(\Omega r)^2}$$

This implies that the induced axial velocity produced by the blade element is aV and the azimuthal velocity is -b

$$\Omega$$

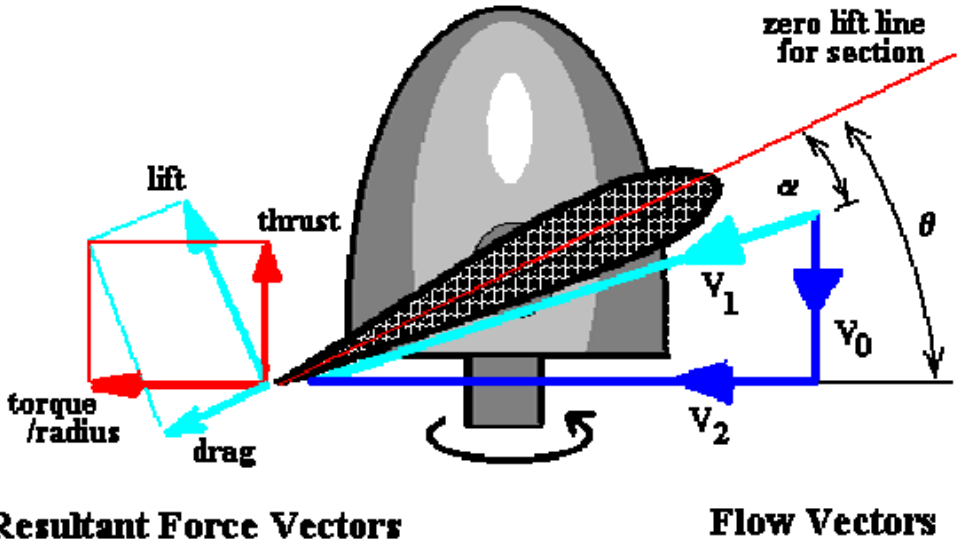

Fig.2 Definition of flow and force directions on a blade element (from ref.1)

r The angle made by the resultant velocity with propeller plane is called the inflow angle

$$\phi$$

, such that

$$\tan\phi = \frac{(1+a)V}{(1-b)\Omega r}$$

$$\sin\phi = \frac{(1+a)V}{V_R}$$

$$\cos\phi = \frac{(1-b)\Omega r}{V_R}$$

Thus, if we know the inflow angle we can easily find the induction factors and finally the resultant velocity at any blade element. We calculate these factors at a blade element which we assume to be independent of other blade elements and the lift generated by this element will only depend on the relative velocity of the wind that strikes it.

1.2.1.1 Momentum Theory

The aim of momentum theory is to find the radial distribution of the inflow angle. As stated, propeller geometry is not important for this. We assume a static disk and define the pressure and air velocities above and below the disk area to derive thrust and torque equations. Assume the pressure just above the disk is

$$p_1$$

and just below the disk

$$p_2$$

with the total area of disk A. Thus the thrust T experienced by the disk will be given by

$$T = A(p_2 - p_1) \tag{1.1}$$

According to law of conservation of momentum the thrust imparted by the air on the disk should be equal to the thrust imparted by the disk to the air which could be calculated with air velocities near and far below the disk

$$T = \dot{m}(V_s - V) \tag{1.2}$$

here

$$\dot{m}$$

is the mass transfer rate and

$$V_s$$

is the velocity far downstream of disk.

$$\dot{m} = \rho V_0 A \tag{1.3}$$

$$p_2 - p_1 = \rho V_0 (V_s - V) \tag{1.4}$$

Since the flow is considered streamline we can apply Bernoulli equation, for the upward region of the disk

$$p_0 + \frac{1}{2}\rho V^2 = p_1 + \frac{1}{2}\rho V_0^2 \tag{1.5}$$

and for the downward region

$$p_2 + \frac{1}{2}\rho V_0^2 = p_0 + \frac{1}{2}\rho V_s^2 \tag{1.6}$$

now combining the two equations

$$p_2 - p_1 = \frac{1}{2}\rho (V_s^2 - V^2) \tag{1.7}$$

With previously defined velocity relations

$$V_0 = \frac{1}{2}(V_s + V) \tag{1.8}$$

$$V_0 = V(1 + a) \tag{1.9}$$

Now We divide the disk in small annuli and calculate the thrust produced by each one as

$$\Delta T = \rho V_0 2\pi r \Delta r (V_s - V) \tag{1.10}$$

$$\frac{dT}{dr} = 4\pi\rho r V^2 a(1 + a) \tag{1.11}$$

We can obtain the torque on the elemental disk as

$$dQ = \rho V_0 \cdot 2\pi r dr \cdot 2b\Omega r \tag{1.12}$$

$$\frac{dQ}{dr} = 4\pi\rho r^3 \Omega V_0 b \tag{1.13}$$

We can see that induced factors cannot be calculated by momentum theory alone but if determined , thrust and power can be easily calculated using momentum theory.

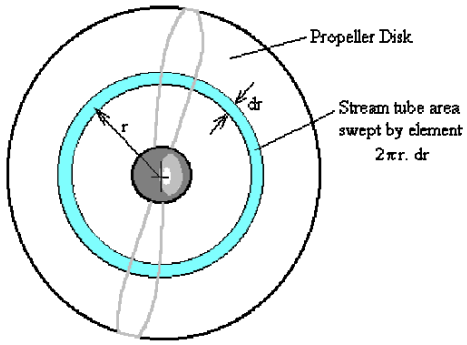

1.2.1.2 Blade Element Momentum theory

As the blade rotates with an angular speed of

$$\Omega$$

, the blade element is subjected to elemental lift and drag forces of dL and dD respectively. The values of those forces are given by

$$\Delta L = \frac{1}{2}\rho V_R^2 C_l c \Delta r \tag{1.14}$$

$$\Delta D = \frac{1}{2}\rho V_R^2 C_d c \Delta r \tag{1.15}$$

And the resultant force on the element is given by

$$dF_R = \sqrt{dL^2 + dD^2} = dL\sqrt{1 + \tan^2\gamma} = dL\sec\gamma \tag{1.16}$$

where gamma is the arctan of cd/cl. The resultant force can be resolved into 2 components, with one component being in the axial direction and the other in the azimuthal direction. The axial component of the force is the same as the elemental thrust force due to a single blade, and if the propeller has B blades then the elemental thrust of the propeller is

$$dT = dL\cos\phi - dD\sin\phi = \frac{1}{2}\rho V_R^2 B c dr(C_l\cos\phi - C_d\sin\phi) \tag{1.17}$$

$$dT = \frac{1}{2}\rho V_R^2 B c C_l dr(\cos\phi - \tan\gamma\sin\phi) \tag{1.18}$$

The azimuthal component of the elemental resultant force when multiplied by the radial distance, r, is the elemental torque of the propeller.

$$\frac{dQ}{dr} = \frac{1}{2}Bc\rho V_R^2 C_l r\sec\gamma\sin(\phi + \gamma) \tag{1.19}$$

Now that we have thrust and torque equation by two different methods and we can compare the two equations and solve for the inflow angle phi

The thrust equation can be written as

$$aV = \frac{1}{4}\sigma C_l \sec\gamma \csc\phi \cos(\phi+\gamma) V_R \tag{1.20}$$

Similarly, the equation for torque gives the following result

$$b\Omega r = \frac{1}{4}\sigma C_l \sec\gamma \csc\phi \sin(\phi+\gamma) V_R \tag{1.21}$$

We can write the equation for axial velocity as

$$V_R \sin\phi = V + \frac{1}{4}\sigma C_l \sec\gamma \csc\phi \cos(\phi+\gamma) V_R \tag{1.22}$$

on further simplifying it we can write it as a function of inflow angle

$$F(\phi) = \frac{V}{V_R} = \sin\phi - \frac{1}{4}\sigma C_l \sec\gamma \csc\phi \cos(\phi+\gamma) \tag{1.23}$$

$$V_R \cos\phi = \Omega r - \frac{1}{4}\sigma C_l \sec\gamma \csc\phi \sin(\phi+\gamma) V_R \tag{1.24}$$

$$G(\phi) = \frac{\Omega r}{V_R} = \cos\phi + \frac{1}{4}\sigma C_l \sec\gamma \csc\phi \sin(\phi+\gamma) \tag{1.25}$$

$$g(\phi) = (\Omega r \sin\phi - V\cos\phi)\sin\phi - \frac{1}{4}\sigma C_l \sec\gamma(\Omega r \cos(\phi+\gamma) + V\sin(\phi+\gamma)) \tag{1.26}$$

The equation is a transcendental equation in

$$g(\phi)$$

that can be solved for the required value of phi. This equation must be solved numerically as an iterative method. Out of the several iterative methods we are using the regual falsi method to determine inflow angle at each blade element. After we get the inflow angle, we can easily calculate the thrust and torque as

$$\frac{dT}{dr} = \frac{1}{2}Bc\rho V_R^2(\phi)\left[C_{l,\alpha}\alpha\cos\phi - C_d(\alpha)\sin\phi\right] \tag{1.27}$$

$$\frac{dQ}{dr} = \frac{1}{2}Bc\rho V_R^2(\phi)\left[C_{l,\alpha}\alpha\sin\phi + C_d(\alpha)\cos\phi\right] r \tag{1.28}$$

Once we have the elemental thrust and torque we just need to integrate it over the span to obtain total thrust and torque experienced by the propeller

$$T = \Delta R\left[\frac{1}{2}\left(\frac{dT}{dr}\right)_1 + \sum_{n=2}^{N}\left(\frac{dT}{dr}\right)_n\right] \tag{1.29}$$

$$Q = \Delta R\left[\frac{1}{2}\left(\frac{dQ}{dr}\right)_1 + \sum_{n=2}^{N}\left(\frac{dQ}{dr}\right)_n\right] \tag{1.30}$$

Further the empirical corrections like prandtl's tip loss factor and glauert correction can be introduced to account for tip losses and critical axial induction factor. For the Blade Geometry we can optimize the power for certain thrust by keeping a linear twist along the blade according to [3].

1.2.2 Validation using Computational Fluid Dynamics

In this section, we mainly focus on the validation part of the propulsion design. Few propulsion models were validated for their performance in the CFD software, namely, ANSYS Student Version 2025. The reference models were obtained using the mathematical methods mentioned in the previous sections. Further sections talk about the model used for CFD simulation, the theory behind the working principle of the model, the meshing settings used, the solver setup, and the post-processing of the simulation results.

1.2.2.1 Introduction to the Virtual Blade Model

The Virtual Blade Model (VBM) in ANSYS Fluent [4] is a simplified aerodynamic representation of rotating propellers or rotors, wherein the model works separately on the fluid domain in which the propellers rotate, simulating the effects of rotating propeller blades, hence eliminating the need for explicit blade geometry. It models the time-averaged effects of the rotating blades on the fluid domain by introducing some source terms in the momentum equations. This model is based on the Actuator Disk Theory, in which the propeller domain is represented by an infinitely thin, permeable disk.

In general CFD simulations, the aircraft is assumed to be stationary and immersed in a moving airstream, hence calculations in reference to the absolute frame of reference are possible. But in VBM, three different frames of reference are required, since firstly, the blades can be best defined in the relative frame of reference about their axis of rotation, the radial direction along the blade and the azimuthal angle.

In VBM, to compute the forces acting on a blade section, it is necessary to transform the velocity field computed in the absolute frame of reference to the local blade section frame of reference to obtain the relative velocity field, hence leading to the need for a third frame of reference that is defined by the tangential velocity vector of the blade section and the normal vector of the propeller disk. Blade airfoil data, per blade section, is then used to calculate the local C_L and C_D values, from which instantaneous propeller forces per unit span can be computed in the form:

$$f_{L,D} = C_{L,D}(\alpha, Ma, Re) \cdot c\left(\frac{r}{R}\right) \cdot \frac{1}{2}\rho V_{\text{rel}}^2 \tag{1.31}$$

Here, c is the function of chord length in terms of r/R, and V_{rel} is the instantaneous relative airflow velocity experienced by each blade cross-section in the frame of reference of the propeller. For a time-averaged solution in the absolute frame of reference, the forces must be time-averaged over one rotation, i.e. geometrically over an angle of 2π. Therefore, the time-averaged forces on the cell faces with face area (ΔA) on the actuator disk become:

$$F_{L,D}\big|_{\text{cell}} = N_b \frac{\Delta A}{2\pi r} f_{L,D} \tag{1.32}$$

Where N_b is the number of blades, and r is the radial coordinate of the cell centre on the disk. This force vector F is further transformed into a vector in the absolute frame of reference of the flow field, namely F'. This is done to include the force in airflow calculations. Therefore, the time-averaged source term per unit cell volume is:

$$S'_{\text{cell}} = \frac{F'_{\text{cell}}}{V_{\text{cell}}} \tag{1.33}$$

This is the source term that is added in the momentum equations in each cell attached to the actuator disk. Once the above source term is computed, the iterative procedure of solving the flow field is done until the input convergence criteria are met. The propeller performance is controlled by the thrust and moment coefficients, given by:

$$C_T = \frac{T}{C_{\text{NA-EU}}\rho V_{\text{tip}}^2 \pi R^2} \tag{1.34}$$

$$C_{M_x} = \frac{M_x}{C_{\text{NA-EU}}\rho V_{\text{tip}}^2 \pi R^3} \tag{1.35}$$

$$C_{M_y} = \frac{M_y}{C_{\text{NA-EU}}\rho V_{\text{tip}}^2 \pi R^3} \tag{1.36}$$

In Fluent VBM, the $C_{(NA-EU)}$ is set to 1.

1.2.2.2 Model Assumptions

- The disk is treated as an axisymmetric discontinuity moving through the fluid.
- The disk has zero thickness but finite area A.
- Thrust and velocity are uniformly distributed over the disk. Time-independent flow conditions.
- Pressure far upstream and downstream equals atmospheric pressure.
- Neglects unsteady blade-wake interactions.

1.2.2.3 Advantages of using the model

- VBM significantly reduces the computational cost by eliminating the need for a fine dynamic mesh around a propeller blade surface, leading to faster simulations compared to fully resolved blade simulations.
- VBM enables a Full-System simulation by allowing easier coupling of aerodynamic components with the propulsion component.
- Smooth integration with actuator or BEMT data.

1.2.2.4 CFD Setup for Propeller Simulation

Fluent VBM adds momentum source terms for each cell of the propeller disk. These cells can be created as a one-cell-thick actuator disk embedded in the mesh, under the mode of Embedded Disk Mode (EDM) or can be mapped to a floating disk surface that cuts the geometry, under the mode of Floating Disk Mode (FDM).

If EDM is used, an internal surface at the propeller location should be created in the flow domain. It should further be classified as an internal wall, which will be discretised by a single layer of nodes. Note that a single layer of prism or hexahedral cells can be attached to the disk surface.

When using FDM, there is no need to create a separate propeller disk in the geometry. Instead, the general geometry of the fuselage can be created and then later on from the VBM GUI in Fluent, a floating disk can be generated at the specified coordinates of the specified dimensions.

Geometry and Meshing

The Virtual Blade Model operates on the blade geometry that can be represented as a stack of 2D airfoils that can vary in chord length, twist and geometry along the normalised blade span r/R in sections. Here, VBM can determine the local Reynolds number and Mach number and can further interpolate local C_L and C_D values. For the first CFD analysis test case, a standardised mesh with specified blade geometry is being used.

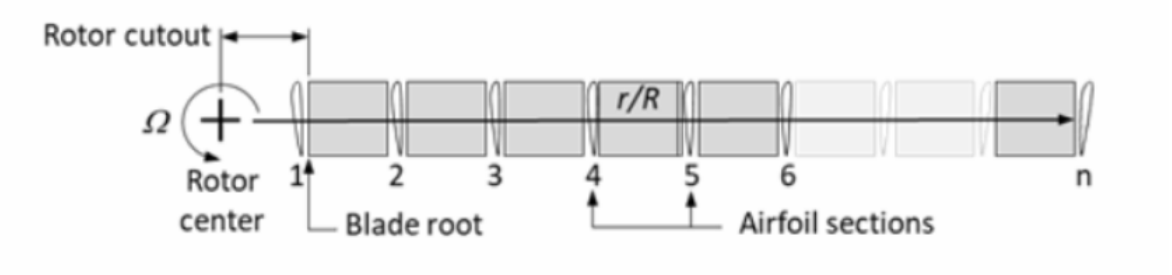

Section	r/R	Chord [m]	Twist [deg]	Airfoil
0	0.30	0.100000	0.00000	naca16016
1	0.40	0.098922	-6.55173	naca16016
2	0.50	0.095905	-12.11207	naca16016
3	0.60	0.090733	-17.06897	naca16016
4	0.70	0.083621	-21.16379	naca16016
5	0.80	0.074353	-24.91379	naca16016
6	0.90	0.063308	-28.53448	naca16016
7	0.95	0.056519	-30.99138	naca16016
8	1.00	0.050000	-35.12931	naca16016

Table 1.1: Blade geometry data: sectional parameters for the VBM propeller model.

Since, we used the Embedded Disk approach in our simulation, we will be talking about the meshing guidelines about the same. As mentioned before, a single layer of prism or hexahedral cells should be extruded from the cell faces attached to the disk. Although there is no definitive rule regarding the thickness of these cells, it is recommended that the layer remain between $1/40th$ to $1/100th$ of the diameter of the disk. The live or free stream region can have a relatively coarser mesh setup to reduce the computational requirements. A single prismatic cell layer in the downstream direction of the disk should be marked as the disk region. This will be a separate fluid domain, and its role is to improve the meshing quality near the disk region as well as to provide a transition from the actuator disk to the free stream airflow domain. The propeller disk region is crucial is capturing the complex effects of momentum change imparted by VBM. Furthermore, it should be ensured that the mass flow through the inlet and outlet is much larger than the mass flow through the propeller disk to avoid diverging results or poor convergence.

1.2.2.5 Airfoil File Format

The accuracy of the simulation results depends directly on the quality of the lift and drag data supplied for each blade section. Since the blade is constructed by stacking airfoils, multiple airfoils can be used to define the blade profile. As the local flow velocity varies along the blade radius, the supplied data must include lift and drag coefficients across a wide range of Reynolds and Mach numbers sufficient to cover the operating conditions encountered.

Furthermore, the data must include the coefficient variation over the full angle-of-attack range, $-180° < \alpha < 180°$, to account for all possible flow regimes including stall and reverse flow conditions.

An example of the required airfoil data format is shown below:

```
naca0015  (Name of the airfoil; same as the airfoil file name, 30 characters maximum)
2          Total number of Cl and Cd tables in the file (maximum 25 tables combined)
cl         Label at the beginning of the Cl table (10 characters maximum)
100000.0   Reynolds number of the table
0.1        Mach number of the table
41         Number of lines in the subsequent table
-180.00  0.0000   Angle of attack (deg) and Cl values
-172.00  0.7800
 :
  0.00   0.0000
 :
 172.50 -0.7800
 180.00  0.0000
cd         Label at the beginning of the Cd table (10 characters maximum)
100000.0   Reynolds number of the table
0.1        Mach number of the table
71         Number of lines in the subsequent table
-180.00  0.0220   Angle of attack (deg) and Cd values
-175.00  0.0620
 :
  0.00   0.0088
 :
 175.00  0.0620
 180.00  0.0220
          Repeat if additional Cl and Cd tables are available
```

1.2.2.6 Solver setup

The solver setup for this simulation involves configuring the following parameters:

- **Units:** The units used in this simulation are SI units (m, kg, s, deg).
- **Operating Conditions:** The operating pressure is set to $101325\ \mathrm{Pa}$, and the reference pressure location is at $(-1,\ 0,\ 0)\ \mathrm{m}$.
- **Physics:**
  - **General:**
    - Type = Pressure-Based
    - Velocity Formulation = Absolute
    - Time = Steady (VBM enables steady-state analysis)
  - **Energy Model:** Disabled
  - **Solver Model:** Spalart–Allmaras (1-equation) turbulence model

The Spalart–Allmaras model is a one-equation turbulence model developed specifically for aerodynamic and external flows. It solves a single transport equation for a modified turbulent kinematic viscosity, making it computationally efficient and less expensive than the two-equation models such as k–ω or k–ε.

The governing equation for the model is:

$$\frac{\partial(\rho\tilde{\nu})}{\partial t} + \frac{\partial(\rho u_j \tilde{\nu})}{\partial x_j} = G_{\tilde{\nu}} + \frac{1}{\sigma_{\tilde{\nu}}}\left[\frac{\partial}{\partial x_j}\left((\mu + \rho\tilde{\nu})\frac{\partial\tilde{\nu}}{\partial x_j}\right)\right] - Y_{\tilde{\nu}} \tag{1.37}$$

where:

- $\tilde{\nu}$ = modified turbulent viscosity (model variable)
- ρ = density
- u_j = velocity components
- μ = molecular viscosity
- $G_{\tilde{\nu}}$ = production term
- $Y_{\tilde{\nu}}$ = destruction (dissipation) term
- $\sigma_{\tilde{\nu}}$ = turbulent Prandtl number for $\tilde{\nu}$

The **Strain/Vorticity-Based production** option is enabled to prevent false turbulence generation in a rotating reference frame, thereby improving predictions in rotating and swirling flows. Additionally, the **Curvature Correction** feature is enabled, which introduces a correction function that scales turbulence production based on local curvature effects.

Materials

- **Fluid:** Air
- **Density:** Ideal-gas formulation

Boundary Conditions

- **Inlet:** Velocity $\mathbf{V}_{\text{in}} = (20,\ 0,\ 0)\,\mathrm{m/s}$, with turbulence viscosity ratio set to 1.
- **Outlet:** Gauge pressure $= 0\,\mathrm{Pa}$, using Absolute Backflow Reference Frame. Backflow modified turbulent viscosity $\tilde{\nu}_{\text{bf}} = 0.0001\,\mathrm{m^2/s}$ (default).
- **Walls:** The “outer” boundary is assigned with shear condition **Specified Shear** $(0, 0, 0)$ for X, Y, and Z components.

Reference Values

The reference values are computed from the **inflow** region, with the following parameters:

Quantity	Value
Area	$0.785398\,\mathrm{m}^2$
Length	$0.05\,\mathrm{m}$
Density	$1.225\,\mathrm{kg/m}^3$
Enthalpy	$0\,\mathrm{J/kg}$
Pressure	$0\,\mathrm{Pa}$
Velocity	$20\,\mathrm{m/s}$
Viscosity	$1.7894 \times 10^{-5}\,\mathrm{kg/(m \cdot s)}$
Ratio of Specific Heats	1.4
Y^+ for Heat Transfer Coefficient	300
Reference Zone	`live`

Table 1.2: Reference values for the VBM simulation.

Solution Methods

Setting	Scheme / Option
Scheme	Coupled
Gradient	Green–Gauss Node Based
Pressure	PRESTO!
Density	Second Order Upwind
Momentum	Second Order Upwind
Modified Turbulent Viscosity	First Order Upwind
Energy	Second Order Upwind
Pseudo Time Method	Global Time Step

Table 1.3: Solution method configuration.

Solution Initialization

Standard initialization is performed and computed from the **inflow**, using the **Absolute Reference Frame**.

VBM Rotor Inputs

The following settings define the configuration for the **VBM Embedded Disk Mode (EDM)** used in this study.

1.2.2.7 VBM Field variables

VBM computes and provides 15 VBM data fields for each computational cell in the entire domain. The VBM variables are cell-based and will not display correctly as node variables. They are calculated only in the cells attached to the actuator disks. The labels of the VBM parameters are listed in 1.2.2.7

Variable Name	Description
VBM Radius	Radius
VBM Incident Velocity	Airflow relative incident velocity
VBM Pitch Angle	Effective pitch angle (as defined in Blade Pitch)
VBM Chord	Blade chord
VBM Reynolds Number	Reynolds number
VBM Mach Number	Mach number
VBM AoA	Angle of attack
VBM cl	Lift coefficient
VBM cd	Drag coefficient
VBM Normal Force	Normal component of instantaneous rotor force
VBM Tangential Force	Tangential component of instantaneous rotor force
VBM Radial Force	Radial component of instantaneous rotor force
VBM X-Force	x-component of time-averaged force $(F'_{L,D})$
VBM Y-Force	y-component of time-averaged force $(F'_{L,D})$
VBM Z-Force	z-component of time-averaged force $(F'_{L,D})$

Table 1.4: Description of Virtual Blade Model (VBM) output variables.

1.2.2.8 VBM Output and Post-processing

The VBM outputs include the force,moment and power of the rotor disk, evaluated using blade element theory (BET) as given in 1.2.2.8 , considering the local coordinates x'y'z' shown in 1.1

Output Type	**Definition – Quantity**	**Definition – Coefficient**
Xp-force (N)	$\mathcal{F}_{x'} = \sum F_{x'}$	$C_{F_{x'}} = \dfrac{\mathcal{F}_{x'}}{\rho_{\text{ref}} V_t^2 A_d}$
Yp-force (N)	$\mathcal{F}_{y'} = \sum F_{y'}$	$C_{F_{y'}} = \dfrac{\mathcal{F}_{y'}}{\rho_{\text{ref}} V_t^2 A_d}$
Thrust (N)	$T = \sum F_{z'}$	$C_T = \dfrac{T}{\rho_{\text{ref}} V_t^2 A_d}$
Roll-moment (N·m)	$M_{x'} = \sum F_{z'} \cdot y'$	$C_{M_{x'}} = \dfrac{M_{x'}}{\rho_{\text{ref}} V_t^2 A_d R}$
Pitch-moment (N·m)	$M_{y'} = \sum F_{z'} \cdot x'$	$C_{M_{y'}} = \dfrac{M_{y'}}{\rho_{\text{ref}} V_t^2 A_d R}$
Torque (N·m)	$Q = \sum F_t \cdot r$	$C_Q = \dfrac{Q}{\rho_{\text{ref}} V_t^2 A_d R}$
Power (W)	$P = Q \cdot \Omega$	$C_P = \dfrac{P}{\rho_{\text{ref}} V_t^3 A_d}$

Table 1.5: VBM output definitions: quantities and coefficients.

In the table, x',y'and z' represent the local coordinates and r stands for the radius of a facet cell. The components of the time-averaged force on the facet cell are denoted as F'_x, F'_y, F'_z and F_t represents the tangential force on the facet cell. Within this table, $V_t = R\Omega$ is the rotor speed, $A_d = \pi R^2$ is the rotor disk area, R is the rotor radius and Ω is the rotational speed of the rotor.

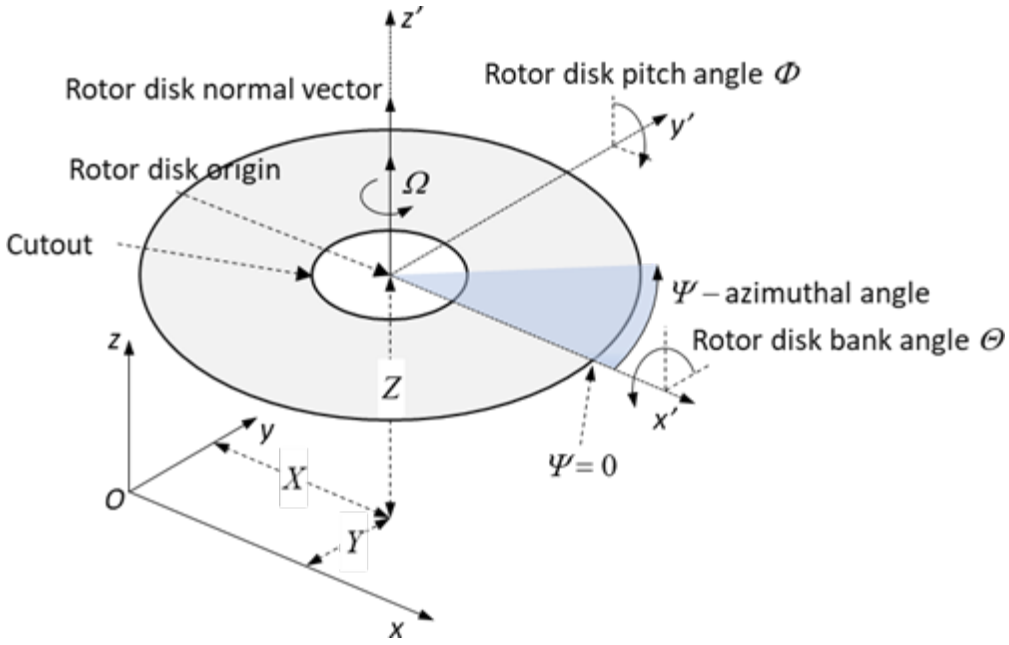

Figure 1.1: Blade schematic

For the post processing we create a cutting plane through the wake of a propeller to visualize the momentum changes produced by the actuator disk. The cutting plane will allow us to compare the effect of trimming on the solution. This cutting of planes is also done in the rotor zone, parallel to the disk, such that it cuts all prismatic elements in the rotor zone (disk). This cutting plane will be used to visualize the VBM data distributions on the disk.

1.3 EDF

Electric Ducted Fans are common Thrust Plants used in various kinds of aircrafts, but in our application, they have limited efficacy. From a technical point of view, the wetted area and geometric interferences of the duct add a lot of drag to the aircraft. They need to be designed specifically for the cruise conditions for improved system efficiency, that too at a higher airspeed, but only with reduced low-speed performance. This also acts as an additional component to be manufactured, with tight tolerances between the blade tip and internal surface, adding manufacturing and maintenance costs. EDFs also have a high disk loading, added weight and mechanical complexity. Internal flow in EDFs may be harder to inspect and repair.

EDFs also have certain advantages over a propeller, including a higher thrust production, reduced noise and added safety. If cruise speed is relatively high (not our case!), EDFs start to be competitive as flight speed climbs into higher ranges where the duct can reduce tip losses and the fan operates closer to its design point.

Thus for our Distributed Electric Propulsion (DEP) STOL, the winner in general is propellers - ideally many low-disk-loading, slow-turning propellers that blow the wing and flaps. EDFs may work, but they are generally worse for the low-speed high-static-thrust regime STOL needs.

Chapter 2

Wing

2.1 Introduction

The Wing can undoubtedly be considered as one of the most important components for an STOL aircraft. Without an optimally designed wing, it is impossible to achieve high performance indices with any amount of thrust. Particularly in a STOL aircraft, a very high Coefficient of Lift C_L is required for the takeoff scenario, since our desire of shorter runway lengths leads to a lesser takeoff velocity for the aircraft.

In this Chapter, we have covered 3 basic scenarios of wings, which improve the coefficient of lift incrementally. We start with a simple infinite wing with an airfoil like the NACA 2412. The high coefficients of lift desired for an STOL cannot be obtained by just using an optimal airfoil. For achieving higher lift, we will also be introducing flaps - which are the most common way of enhancing the lift. Further enhancements can be done by using the jet induced by our propulsion system and blowing it onto the wing and flap surface.

2.2 Wing Without Flaps

2.2.1 Overview

In this section, our aim is to solve the coefficient of lift for a cambered airfoil. We do this through the implementation of the thin airfoil theory and the vortex sheet method. We use this method because it allows us to solve and hence compare the change in the coefficient of lift in the case of a blown flap later on.

2.2.2 Mathematical Model

In the vortex sheet method, we consider the airfoil to be made up of a series of vortices that form along the camber of the airfoil. This assumption allows us to calculate the circulation over the airfoil, which further allows us to calculate the lift and the coefficient of lift of the airfoil.[5]

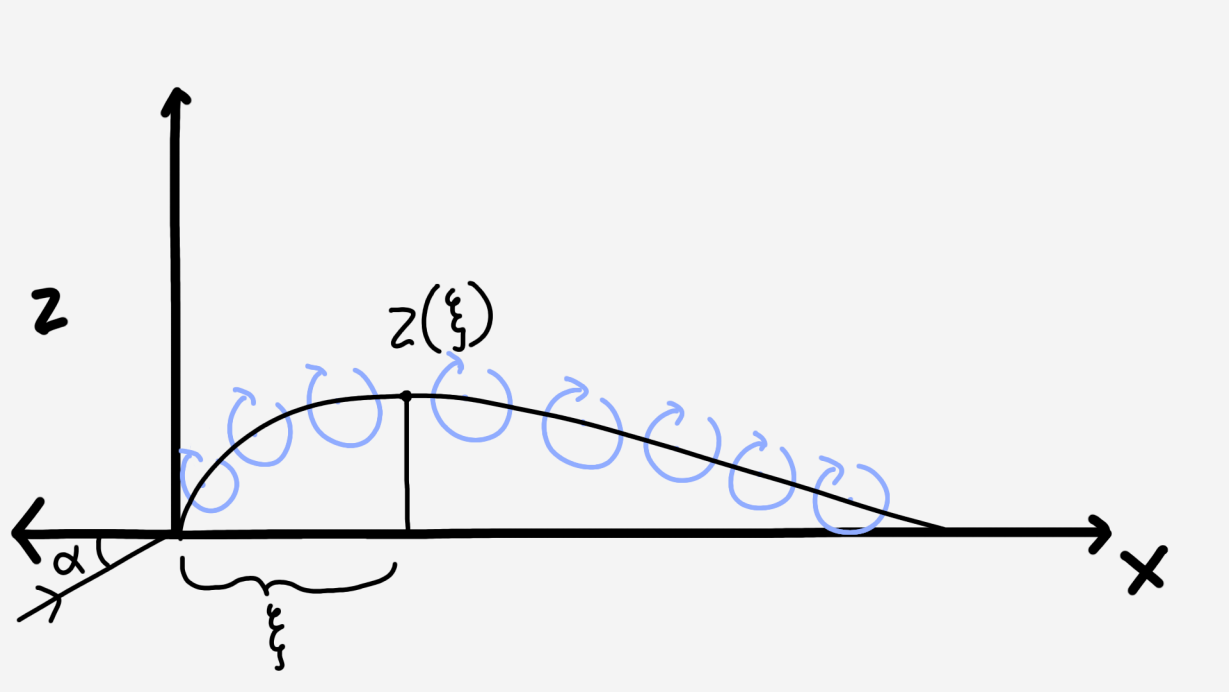

Before starting our analysis, we are going to take certain assumptions so that we can arrive at a fairly accurate result with lesser complexity. We will assume that the airfoil to be thin and that we would operate at a small angle of attack α. We will also consider the wingspan to be infinite as we are mainly focusing on the 2D analyis of the airfoil.

Now, we take the flow of air normal to the airfoil to be 0. Mathematically, this looks like

$$V_{\infty,n} + \omega'(s) = 0 \tag{2.1}$$

Where $V_{\infty,n}$ is the component of the free stream velocity that is normal to the camber at some point s on the camber. The other term, $\omega'(s)$, represents the contribution of the vortex sheet to the normal component of the velocity to the camber line. We find the term $V_{\infty,n}$ where we take the components of the free stream velocity normal to the camber using the angle of attack as well as the angle of the camber. In this we use small angle approximations to consider $sin(\theta) \approx \theta$ and $tan^{-1}\theta \approx \theta$

$$V_{\infty,n} = V_{\infty}(\alpha - \frac{dz}{dx}) \tag{2.2}$$

We add the definition for ω as

$$\omega(x) = -\frac{1}{2\pi}\int_0^c \frac{\gamma(\xi)\,d\xi}{(x-\xi)}. \tag{2.3}$$

Where $\gamma(\theta)$ is the vortex strength. Finally, we put this equation in equation 2.1 and we get -

$$V_{\infty}(\alpha - \frac{dz}{dx}) = -\frac{1}{2\pi}\int_0^c \frac{\gamma(\xi)\,d\xi}{(x-\xi)}. \tag{2.4}$$

We perform a change of basis for x and ξ so that our calculation becomes easier.

$$x = \frac{c}{2}(1 - \cos\theta_0) \textbf{ and } \xi = \frac{c}{2}(1 - \cos\theta) \tag{2.5}$$

Applying these transforms to the equation 2.4, we get -

$$\frac{1}{2\pi}\int_0^\pi \frac{\gamma(\theta)\sin\theta d\theta}{\cos\theta - \cos\theta_0} = V_\infty\left(\alpha - \frac{dz}{dx}\right). \tag{2.6}$$

Due to the presence of regions where the above equation is undefined, it is not directly solvable. So to solve this, we approximate this using the Glauert's method of solution [6]-

$$\gamma(\theta) = \frac{V}{\pi}\{A_0\cot\tfrac{1}{2}\theta + A_1\sin\theta + A_2\sin 2\theta + A_3\sin 3\theta + \ldots\}, \tag{2.7}$$

We notice that in this, the Kutta condition has been already applied at all points on the airfoil, so we do not need to make any other conditions to enforce the Kutta condition. This equation can be simplified to -

$$\gamma(\theta) = 2V_\infty\left(A_0\frac{1+\cos\theta}{\sin\theta} + \sum_{n=1}^{\infty} A_n\sin n\theta\right) \tag{2.8}$$

Next, we apply equation (2.8) back to the equation 2.6 and arrive at -

$$\alpha - \frac{dz}{dx} = A_0 - \sum_{m=1}^{\infty} A_m\cos m\theta \tag{2.9}$$

In this we must find the values of A_0 and A_n. To do this, we apply a similar method to what we used in equation 2.8. We first integrate both sides of the equation from 0 to π. This gives us just the A_0 term which is as follows -

$$A_0 = \alpha - \frac{1}{\pi}\int_0^\pi \frac{dz}{dx}d\theta_0 \tag{2.10}$$

For the other terms, we multiply both sides by $cos(m\theta)$ and then integrate the solution from 0 to π. This removes the constant term and provides the desired values.

$$A_n = \frac{2}{\pi}\int_0^\pi \frac{dz}{dx}\cos n\theta_0 d\theta_0. \tag{2.11}$$

Now that we have completely defined $\gamma(\theta)$, we can find the circulation Γ over the airfoil, hence the generated lift L'.

$$\Gamma = \int_0^c \gamma(\xi)d\xi = \frac{c}{2}\int_0^\pi \gamma(\theta)\sin\theta d\theta. \tag{2.12}$$

$$L' = \rho_\infty V_\infty \Gamma = \rho_\infty V_\infty^2 c\left(\pi A_0 + \frac{\pi}{2}A_1\right). \tag{2.13}$$

We use this equation of total lift to calculate the coefficient of lift as-

$$c_l = \frac{L'}{\frac{1}{2}\rho_\infty V_\infty^2 c(1)} = \pi(2A_0 + A_1). \tag{2.14}$$

2.2.3 Bringing in the Third Dimension

2.2.3.1 Introduction

Since we have obtained the mathematical model for determining the co-efficient of Lift, for a given airfoil and angle of attack, we intend to extend these results to 3D. The third dimension brings with it a challenge to optimize the geometry and parameters of the wing to generate maximum co-efficient of lift. For this purpose we plan to use OpenVSP. The inspiration to use OpenVSP was obtained from the cited research paper.[7]

2.2.3.2 OpenVSP and VSPAero

OpenVSP- Vehicle Sketch Pad is an open source, parametric aircraft design and simulation software developed by NASA Langley Research Centre. It provides a rapid way to solve our optimization problem. This is because of the fact that OpenVSP is focused on parameter-driven modelling where each component is controlled numerically. OpenVSP includes a built-in analysis module named VSPAero for aerodynamic predictions using Vortex Lattice Method or Panel Method. OpenVSP supports a Python API which helps us set up an iterative construct that is modifiable for all analysis.

2.2.3.3 Geometry Setup in OpenVSP

To start the design of a wing in OpenVSP we need to define a set of geometric parameters. The most fundamental parameters to study are root chord length, tip chord length, span, sweep angle, dihedral angle, twist angle. Each of these parameters plays an important role in the aerodynamic characteristics of the wing. For this study we used the standard NACA2412 Airfoil but the airfoil can be varied. By defining these parameters, we define the setup for our numerical analysis. With the span we can estimate the number and length of each vortex filament on the wind, the chord line aids in placing the control point and vortex for each panel. The airfoil finally defines our camber for the analysis. Thus, a lattice is generated for further analysis.

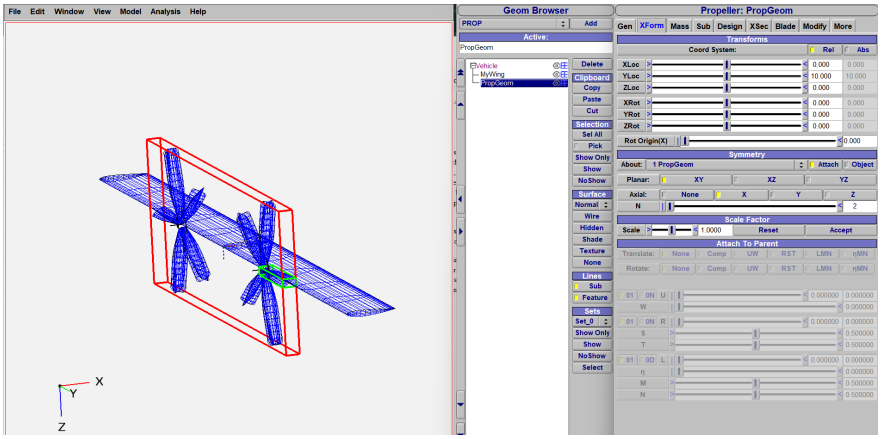

Figure 2.1: Sample GUI of OpenVSP

2.2.3.4 VSPAero

After the geometry has been set up in OpenVSP, we must analyze the aerodynamic characteristics of the wing. This is done by VSPAero. In this we set the method that we want to use (here we have used VLM- thin set shown). We need to set up the number of wake iterations, the angle of attack, sideslip, Mach Number, Reynold's Number and the geometry for the wing. After all the parameters are correctly defined we prepare and launch the solver.

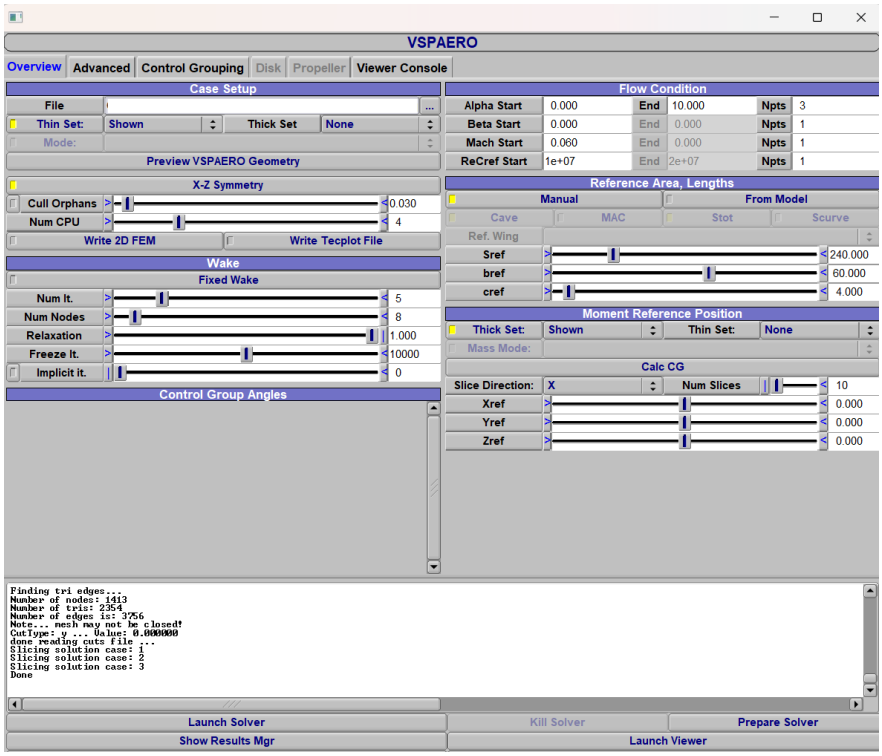

Figure 2.2: Sample GUI of VSPAero

2.2.3.5 Results Manager

Here we obtain all the results and graphs of all the required variables. These can be exported to a .csv file for further analysis.

2.2.3.6 Python API

OpenVSP provides an intricate API to integrate python with OpenVSP. This can be done to test various parameters continuously as described by the user.

2.2.4 Validation using Computational Fluid Dynamics

To prove the accuracy of the mathematical model from the previous section, we ran a Computational Fluid Dynamics (CFD) simulation in Ansys of the same NACA 2412 airfoil

to validate our results. The goal was to use this CFD simulation to generate a C_L vs α curve, which we can then use as a reliable benchmark.

2.2.4.1 Geometry Construction

We began our simulation by first importing the .txt file coordinates of the NACA 2412 airfoil with a chord length (L) of $1m$. After importing this curve in Ansys DesignModeler, we used the ‘rotate‘ function under body transformation. We set this rotation angle as an input parameter (AoA), which allows us to easily re-run the simulation for different angles of attack. For the initial setup, we set $\alpha = 0\,\mathrm{deg}$.

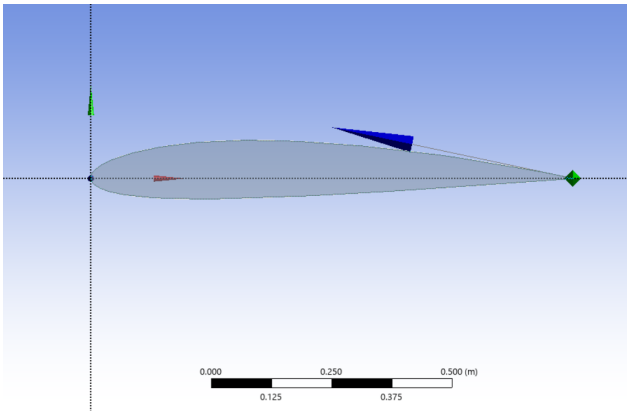

After this, we made an enclosure to simulate the fluid domain. We created a C-shaped domain with a radius of $7.5m$ (15 chord lengths) and a downstream length of $15m$ (15 chord lengths). This size is recommended in CFD literature to ensure the outer boundaries are far enough away ($10 - 20$ chord lengths) to not interfere with the airflow around the wing[8].

We also constructed two vertical lines, one at the trailing edge and another $80mm$ from the leading edge. These lines were used only to split the domain, which helps create a much cleaner, higher-quality structured mesh.

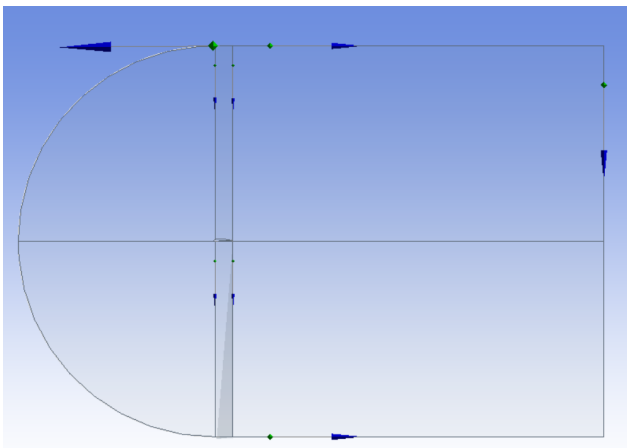

Finally, we performed a ‘Boolean‘ operation to subtract the airfoil shape from the fluid domain. This leaves an "airfoil-shaped hole" which acts as the solid wall. We then changed the property of the enclosure to be a fluid domain.

2.2.4.2 Meshing

To make sure the meshing was done correctly, we started with edge sizing on all edges. We applied a very strong bias factor of 50,000, making the mesh nodes smaller as they get closer to the airfoil.

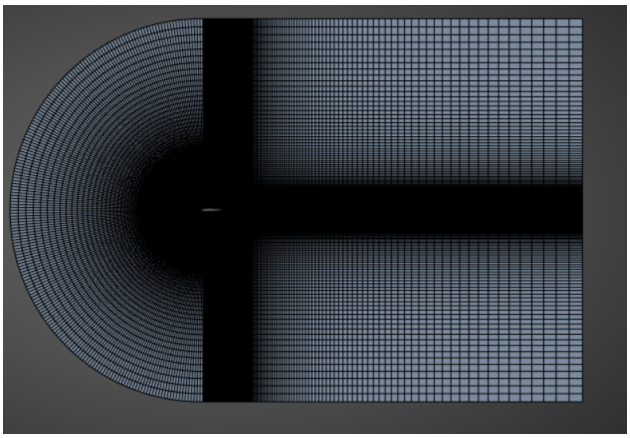

The reason for this is that the area near the airfoil needs to be much finer to get accurate results. Finer mesh is more accurate, but it also takes more computational power. A better approach is to have a mesh that is extremely fine near the airfoil surface (to capture the boundary layer) and gets larger near the outer edges. This gives us accurate results while overall reducing the computational cost.

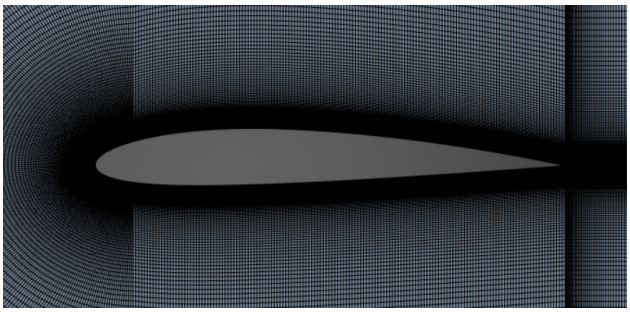

At the end of the meshing step, we created named selections for the $inlet$, $outlet$, and $airfoil$ boundaries, which makes the setup process easier.

2.2.4.3 Y+ Calculation

To ensure our simulation is accurate, we must make sure the first cell height (Δs) is small enough. For the SST $k-\omega$ turbulence model, the non-dimensional wall distance $Y+$ should be ≤ 1 [9].

We calculated the required Δs for our specific boundary conditions:

- Freestream Velocity (V_∞): $20m/s$
- Density (ρ): $1.225kg/m^3$

- Dynamic Viscosity (μ): $1.7894 * 10^{-5} Pa * s$
- Chord Length (L): $1m$
- Desired $Y+$: 1

Using the above conditions, we can calculate:

- **Reynolds Number** $Re_L \approx 1.37 * 10^6$
- **Skin Friction Coefficient** $C_f \approx 0.0032$ *Using 1/7th power-law approximation*.
- **Wall Sheer Stress** $\tau_{wall} \approx 0.784 Pa$
- **Friction Velocity** $V_{fric} \approx 0.8 m/s$
- **Required Cell Height** Δs

$$\Delta s = \frac{Y + * \mu}{V_{fric} * \rho} \approx 1.83 * 10^{-5} m \tag{2.15}$$

After calculating, our desired first layer height is $\approx 1.83 \times 10^{-5} m$. Our model's measured first layer height is $\approx 6.32 \times 10^{-6} m$. Since our actual height is smaller than the required height, our $Y+ < 1$. This confirms that our mesh is good enough for simulation.

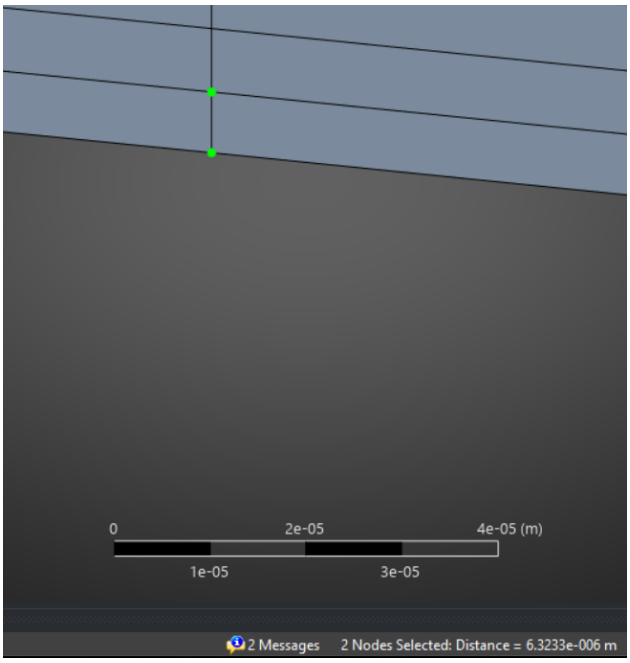

2.2.4.4 Setup

We used standard air properties from the $Y+$ calculation. The solver was set up based on standard practices for this type of aerodynamic simulation.

- **Solver Type:** Pressure-Based, Steady-State.

- **Turbulence Model:** We selected the SST (Shear Stress Transport) $k - \omega$ model. This is the best choice because it accurately predicts flow near the wall (which our $Y+ < 1$ mesh allows) and also handles the freestream flow well.
- **Solution Methods:** We used a Coupled pressure-velocity scheme with Second Order Up - wind discretization for momentum and turbulence. This provides a stable and highly accurate solution.
- **Boundary Conditions:**
  - Inlet: Set as a Velocity Inlet with magnitude $20m/s$. This was applied to the C-shaped arc and the flat top/bottom boundaries.
  - Outlet: Set as a Pressure Outlet with $0Pa$ gauge pressure.
  - Airfoil: Set as a no-slip Wall.
- **Initialization:** We used Hybrid Initialization to get a good starting guess for the solver. We set the convergence criteria for all residuals to 1×10^{-6} to ensure a fully converged solution.

2.2.4.5 Results and Discussion

After running the simulation, we obtained the C_L value for $\alpha = 0\,\mathrm{deg}$ and exported the pressure and velocity contour plots.

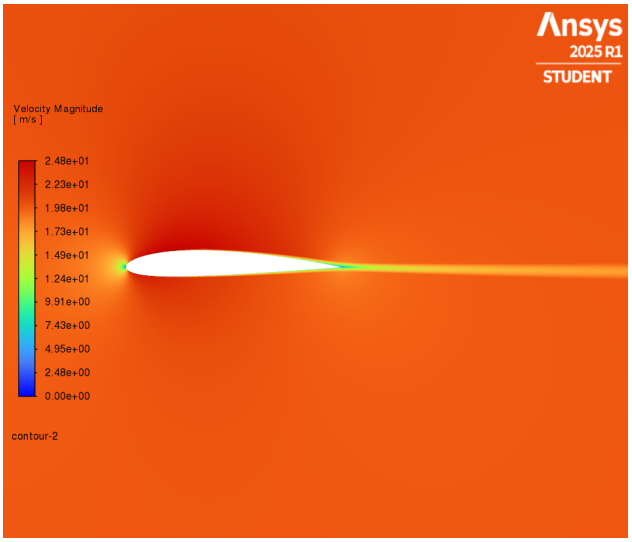

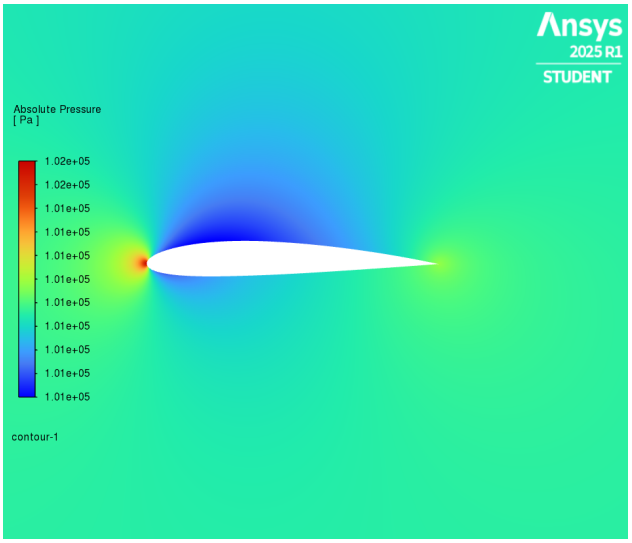

We then used the α parameter we set in the geometry step to automatically re-run the simulation for the following angles of attack: 0, 2, 4, 6, 8, 10, 12, 13, and 15 degrees. The final C_L value for each run was recorded and plotted in the following chart.

Angle of Attack (°)	Lift Coefficient (Cl)
0.0	0.207468
2.0	0.435982
4.0	0.539725
6.0	0.735191
8.0	1.01579
10.0	0.977042
12.0	1.108537
13.0	1.346541
15.0	0.737265

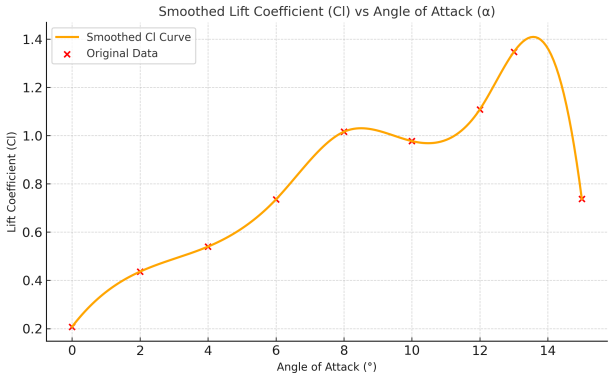

2.2.5 A Comparitive Study

Here we present a comparitive study between the results obtained via the vortex sheet method for 2D airfoil, VLM using OpenVSP and CFD.

Table 2.1: Comparison of Lift Coefficient (C_L)

Angle of Attack (°)	Obtained via Vortex Sheet Method	Obtained via OpenVSP	Obtained via CFD
0.00	0.2341	0.1670	0.2074
2.00	0.4534	0.3855	0.4359
4.00	0.6727	0.6034	0.5397
6.00	0.8921	0.8205	0.7351
8.00	1.1114	1.0364	1.0157
10.00	1.3304	1.2507	0.9770

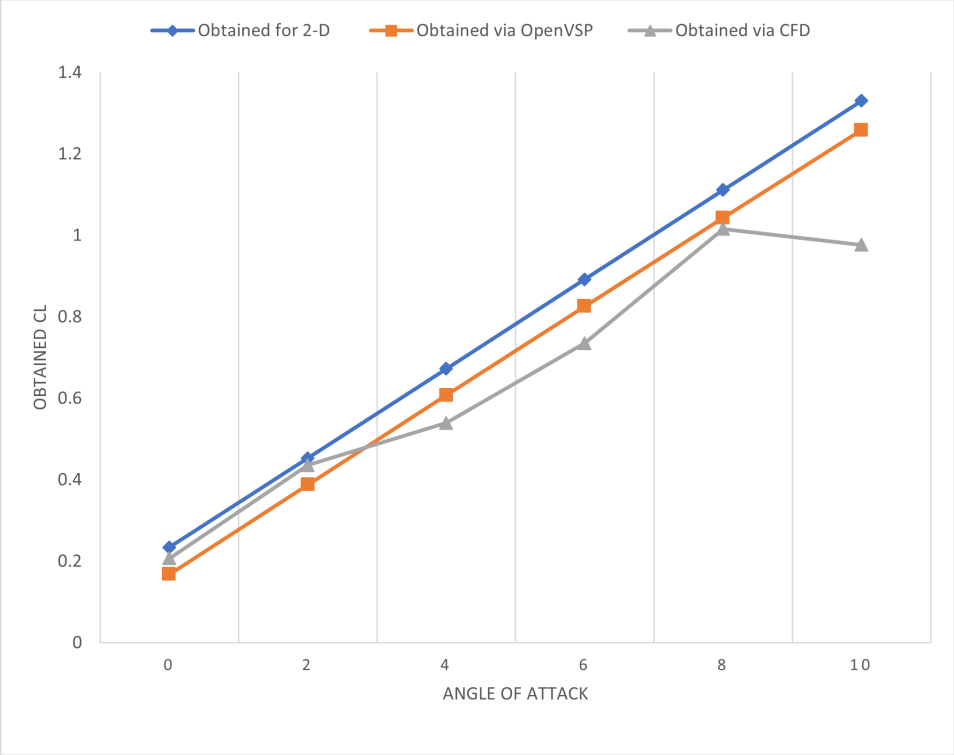

Figure 2.3: Wing geometry designed in OpenVSP using the NACA 2412 airfoil.

The variation of the values observed arise due to the underlying physical modeling assumptions of each method. The 2-d analysis assumes an infinite span whereas VSPAero has a finite span, inducing a downwash and decreasing the angle of attack slightly. Both these method assume inviscid flow at the boundary and neglect viscous effects, thus producing linear curves. CFD on the other hand resolves viscous and 3-D effects, including boundary layer growth and flow separation. Thus, CFD provides the most realistic results among the three.

2.3 Wing With Flaps

2.3.1 Overview

The mathematical techniques used in the previous section are sufficient to include the effects caused by deployment of the flaps. The only modifications required for using the same algorithm will be replacing the shape of the camber with a new shape that replaces the trailing section of the camber with the flap geometry.

2.3.2 Mathematical Model

To obtain this new geometry, we need to deflect a small rear part of the airfoil downward. This is done by adding a deflection to the existing camber. The deflection is a mathematical function that is defined for all the points on the chord, which is zero for all values up to a certain value on the x axis (where the flap starts) and then the deflection can be considered to be a linear function with a constant slope. The slope here would be equivalent to the flap angle.

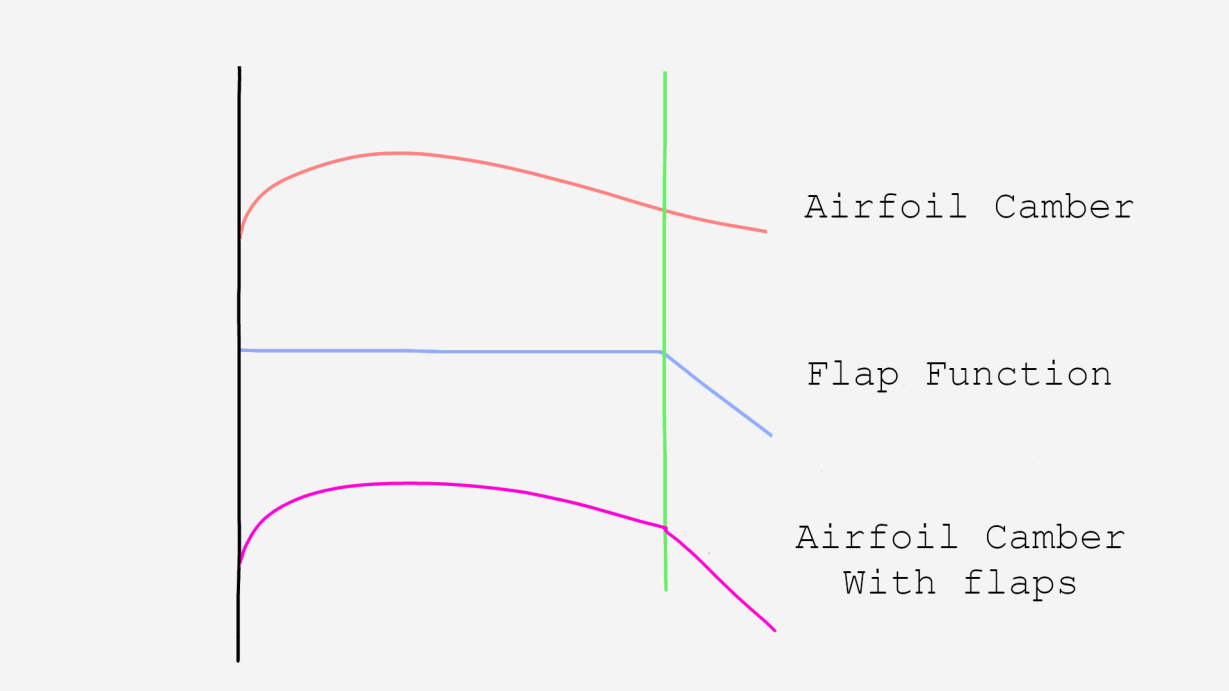

2.3.3 Bringing in the Third Dimension

On OpenVSP we can model the flaps using the Vortex Lattice Method. It offers to insert a sub-surface to the wing where we can control all the parameters related to the flaps. These parameters include the type of subsurface, the position (both spanwise and chord-wise), and the deflection of the surface.

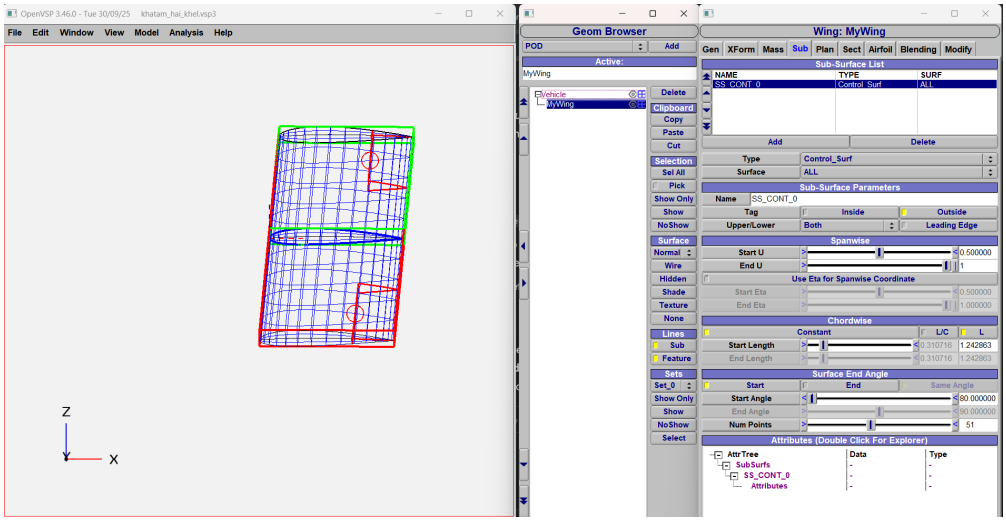

Figure 2.4: Sample GUI for the addition of Flaps in the Wing

Using this method, we can analyze the behavior of the flaps via an iterative construct using python and get the optimum dimensions, position and the deflection. This reduces the effort to be put into rigourous CFD.

2.3.4 Analysis using Computational Fluid Dynamics

Similar Techniques as the previous section would be needed for doing the analysis of a wing with flaps. The only modification will be the wing and flap geometry, as CFD tools can accurately estimate the fluid flow characteristics in these kinds of situations.

2.4 Blown Wing With Flaps

2.4.1 Overview

In his thesis titled "An Assessment of Electric STOL Aircraft", Courtin[10] gives us a good idea of the lift that is produced by an airfoil with a blown flap. However, the result provided in his thesis is limited to a flat airfoil with flaps that provide deflection to the exhaust jet. Since we need to compute the coefficient of lift for a cambered airfoil, we decided to ignore certain assumptions that Courtin[10] made. So, we build upon our existing model to estimate the C_L obtained in the case of wings with blown flaps.

2.4.2 Mathematical Model

Firstly we'll go through the method used by Courtin[10] for calculating the C_L for a flat airfoil. They have assumed an infinite wing with a thin and flat airfoil, and with a jet which is evenly spread over the airfoil such that there is a constant flow of the jet over the entire wingspan. The jet is also approximated as a vortex sheet similar to the airfoil.

We begin by considering that the jet has an inherent curvature $\kappa = d\theta/ds$. We relate this to the velocity change within the jet Δu and average jet velocity u_a as-

$$\Delta u = u_1 - u_2 = u_a \kappa h \tag{2.16}$$

Since the pressure is continuous across the jet boundaries, we consider the pressure difference in the external flow is the same as the pressure difference across the jet. Further, we we use the Bernoulli's equation applied to both the inner flow as well as the jet. This gives with the following equation-

$$\frac{1}{2}\rho(V_1^2 - V_2^2) = \frac{1}{2}\rho_J(u_1^2 - u_2^2) \tag{2.17}$$

We then express this equation in the form of velocity jumps and average velocity as-

$$\rho V_a \Delta V = \rho_J u_a \Delta u = \rho_J u_a^2 \kappa h \tag{2.18}$$

We proceed to write the equation of the wake vortex strength by relating it to the velocity jump as-

$$\gamma_w = \Delta V - V_a \kappa h \tag{2.19}$$

We approximate the average velocity of the jet to be the same as the velocity of the jet at an infinite distance. We continue by defining the jet momentum per unit span as-

$$J' = \int_{-h/2}^{h/2} \rho u^2 dn \approx \rho_J V_J^2 h \tag{2.20}$$

We can write the expression of the vortex strength as-

$$\frac{\gamma_w}{V_\infty} = \frac{J' - \rho V_\infty^2 h}{\rho V_\infty^2} = \frac{\Delta J'}{\rho_\infty V_\infty^2} \tag{2.21}$$

We define a dimensionless coefficient Δc_J, which we will be calling our momentum-excess coefficient.

$$\Delta c_J \equiv \frac{\Delta J'}{\rho_\infty V_\infty^2 c} \tag{2.22}$$

We use this to approximate the vortex strength as-

$$\frac{\gamma_w}{V_\infty} \approx \frac{\Delta c_J}{2} c \frac{\mathrm{d}\theta}{\mathrm{d}x} \tag{2.23}$$

Finally, we use can formulate the equation of the streamline as-

$$\theta(x) \equiv \alpha + \frac{w(x)}{V_\infty} = \alpha + \frac{1}{2\pi}\int_0^c \frac{\gamma(\xi)}{V_\infty}\frac{d\xi}{\xi - x} + \frac{\Delta c_J}{2}\frac{1}{2\pi}\int_c^\infty \frac{d\theta}{d\xi}\frac{d\xi}{\xi - x} \tag{2.24}$$

Assuming a flat and thin airfoil, Spence [11] solved these equations, giving

$$c_\ell = \frac{\partial c_\ell}{\partial \alpha}\alpha + \frac{\partial c_\ell}{\partial \delta_F}\delta_F \tag{2.25}$$

where

$$\frac{\partial c_\ell}{\partial \alpha} = 2\pi(1 + 0.151\sqrt{c_J} + 0.219 c_J) \tag{2.26}$$

$$\frac{\partial c_\ell}{\partial \delta_F} = 2\sqrt{\pi c_J}(1 + 0.151\sqrt{c_J} + 0.139 c_J)^{\frac{1}{2}} \tag{2.27}$$

Now to remove some of these approximations, we have tried a different approach which is similar to the approach that we used to solve the basic thin airfoil.

We start by finding the value of the vortex strength. We cannot use exactly the same method as before 2.7 as this used the fact that the Kutta condition would have to be satisfied. However in the case of the blown flap, the Kutta condition is not satisfied entirely. For this, we divide the vorticity into two regions. One will be the region of the wing ($x < c$), and the other region will be the region after the wing. We consider that the vorticity begins at the trailing edge of the wing and moves downwards eventually combining with the free stream velocity.

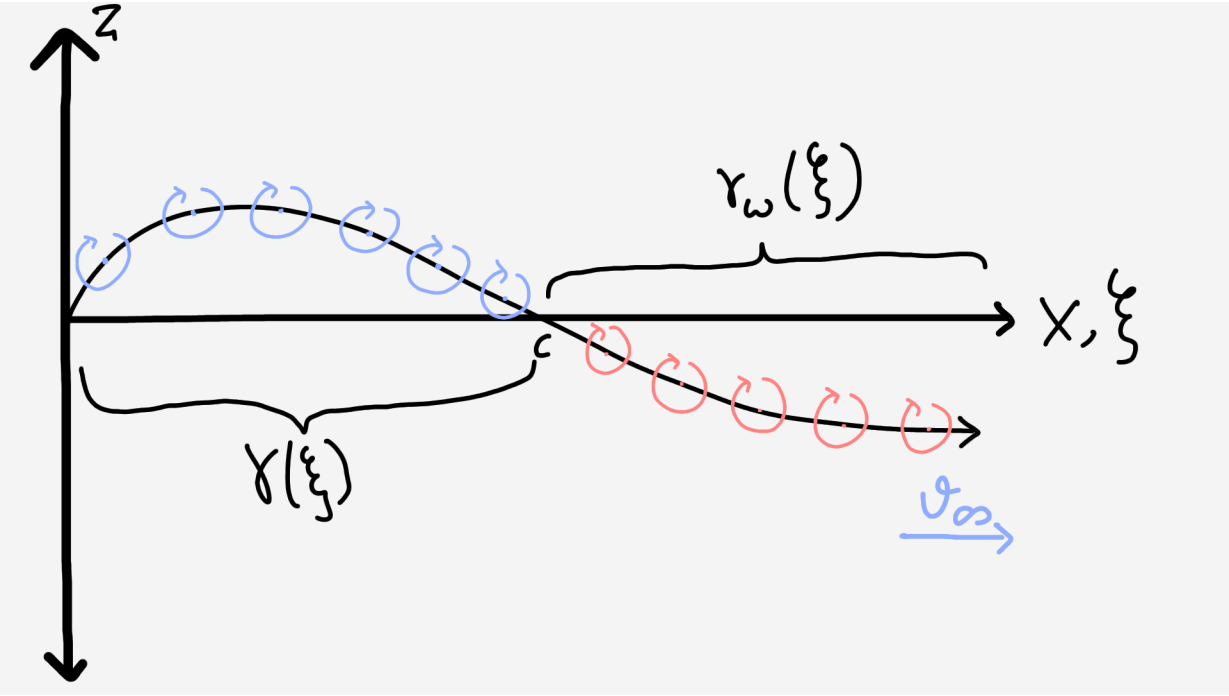

Thus, we expand our gamma as-

$$V_\infty \alpha(\theta) = \frac{1}{2\pi}\int_0^\pi \frac{\gamma(\phi)}{x(\theta)-x(\phi)}d\phi\gamma + \frac{1}{2\pi}\int_c^\infty \frac{\gamma_w(\xi)}{x(\theta)-\xi}d\xi \tag{2.28}$$

In this equation, the $\gamma(\phi)$ term is such that the Kutta condition will be satisfied. Now going back to the equation 2.24, we notice that we can apply the Kutta condition to the $\gamma(x')$ term. To do this, first we rearrange the equation as-

$$\frac{1}{2\pi}\int_0^c \frac{\gamma(\xi)}{V_\infty}\frac{d\xi}{\xi - x} = \theta(x) - \alpha - \frac{\Delta c_J}{2}\frac{1}{2\pi}\int_c^\infty \frac{d\theta}{d\xi}\frac{d\xi}{\xi - x} \tag{2.29}$$

Now we apply the Fourier series simplification 2.7 to the $\gamma(\theta)$ term. We also substitute the value of $\theta(x)$ as the camber line slope since this would be the path of the streamline over the airfoil. This simplifies the equation to-

$$A_0 - \sum_{m=1}^{\infty} A_m \cos m\theta = -\frac{dz}{dx} + \alpha + \frac{\Delta c_J}{2}\frac{1}{2\pi}\int_c^\infty \frac{d\theta}{d\xi}\frac{d\xi}{\xi - x} \tag{2.30}$$

We use similar methods to what we used in our thin airfoil method to get the values of the constants. We start by integrating both sides from 0 to π. This removes all the cos terms meaning that we end up with the equation for the constant A_0. Making all these changes, we end up with the following equation-

$$A_0 = \alpha - \frac{1}{\pi}\int_0^\pi (\frac{dz}{dx})d\theta + \frac{\Delta c_J}{4}\frac{1}{\pi^2}\int_c^\pi \int_0^\infty \frac{d\theta}{d\xi}\frac{d\xi}{\xi - x}d\Theta \tag{2.31}$$

We use the equation 2.5 to change the basis and make the calculations easier.

$$A_0 = \alpha - \frac{1}{\pi}\int_0^\pi (\frac{dz}{dx})d\theta + \frac{\Delta c_J}{2}\frac{1}{\pi^2 c}\int_c^\pi \int_0^\infty \frac{d\theta}{d\theta'}\frac{d\theta'}{cos(\theta) - cos(\theta')}d\Theta \tag{2.32}$$

Similarly, we multiply both sides with $cos(n\theta)$ and we integrate both sides from 0 to π. This Removes the common term from the equation (A_0) and we end up with the following-

$$A_n = -\frac{\Delta c_J}{2}\frac{1}{\pi^2}\int_0^\pi \int_0^\infty \frac{d\theta}{d\xi}\frac{d\xi}{\xi - x}d\Theta + \frac{1}{\pi}\int_0^\pi (\frac{dz}{dx})cos(n\theta)d\theta \tag{2.33}$$

We also change the variable to make things easier

$$A_n = -\frac{\Delta c_J}{\pi^2}\int_0^\pi \int_0^\infty \frac{d\theta}{d\theta'}\frac{d\theta'}{cos(\theta) - cos(\theta')}d\Theta + \frac{1}{\pi}\int_0^\pi (\frac{dz}{dx})cos(n\theta)d\theta \tag{2.34}$$

Now, one of important things in this is defining the function of the jet streamline and how this merges with the free stream velocity. For this, we use the formula given below [12]-

$$\frac{y}{D} = aJ^b\left(\frac{x}{D}\right)^c \tag{2.35}$$

In this,we must find the values of the constants experimentally.

Now to find the coefficient of lift, we use similar methods to what we used before. We first start by defining the circulation which is the same as in equation 2.12. After this, we find the Lift and the coefficient of list which is the same as in equations 2.13 and 2.12. Thus we end up with our final equation as-

$$c_l = \frac{L'}{\frac{1}{2}\rho_\infty V_\infty^2 c(1)} = \pi(2A_0 + A_1). \tag{2.36}$$

Hence, this equation allows us to compute the coefficient of lift for cambered airfoils as well as those airfoils with flaps since we use the same method to deflect the camber of the airfoil to simulate the flap which we had used in the Section 2.3.2.

2.4.2.1 Model Validation and Error Analysis

In this sub section, we will focus on analyzing the error that our numeric gives us over a few cases of wind tunnel testing.

We first verify this against the solution that was stated by Spence [11]

Model Validation for a Symmetric airfoil			
Angle of Attack (degrees)	Flap Deflection (degrees)	C_l Spence	C_l Our Model
0	0	0	0
5	0	0.81050	0.7461
0	5	0.42430	0.5530
5	5	1.234	1.299
7.5	7.5	1.85221	1.9514

From this it is visible that the C_l of the model made my Spence, and the C_l of our model is similar. The small variations may have arises due to a few approximations made in the equation of the jet as well as some approximations made in the size of the flaps. This results are also consistent with those found by Courtin [10]

2.4.2.2 Future Advancements

There can be a lot of improvements made to this model such as better modeling the jet of air that includes the path that the jet follows as it interacts with the free stream velocity downstream as well as the contraction of the jet after it interacts with the propeller. Another change that can be made is the implementation of the $3D$ corrections which allows us to model this for a finite length wing. The calculation of the coefficient of drag is also an important addition that can be made in this model.

2.4.3 CFD

To accurately simulate the blown flap in CFD, the plan is to map the actual velocity profile generated with the Virtual Blade Model (VBM) directly onto the disc inlets. We need to do this because a standard, uniform inlet simply won't suffice for this type of analysis. By using the VBM data, we're essentially forcing the inlets to behave like real propellers, complete with the actual slipstream and swirl patterns. This is crucial because it allows us to accurately capture how that high-velocity air interacts with the wing surface, which is the whole point of the blown flap design. It should give us much more realistic lift and drag numbers than a simplified model would.

Chapter 3

Planned Timeline

Over the next 3 weeks, our work will be focused on further refining the mathematical models by performing rigorous validation using techniques like Computational Fluid Dynamics and by Experimental Testing using Wind Tunnels.

As we refine our models further and further, we'll also work on constraint optimization techniques to achieve the desired targets of Lift Coefficient, L/D ratios, Lift Targets, T/W ratios, and also to identify how our design affect the aircraft's other parameters. This shall be done by obtaining the optimum parameters of the geometry of the wings, propellers, flaps, and their positions relative to each other. Once obtained, these will be verified using CFD.

We will also look into other kinds of unconventional propulsion or wing-designs. Such designs may have been less-explored, but they may hold the key to achieving cost and energy efficient flight, while producing high lift and lesser speeds. They may also add structural strength, or reduce spatial requirements, or provide more eco friendly travel options.

Bibliography

[1] Electra. “Home | electra.aero.” Accessed: 12 November 2025. [Online]. Available: https://electra.aero.

[2] H. Winarto, “Bemt algorithm for the prediction of the performance of arbitrary propellers,”

[3] Leishman, *Principles Of Helicopter Aerodynamics*.

[4] A. Inc. “Ansys fluent 2025 r1 - computational fluid dynamics (cfd) software.” Accessed: 2025-11-12. [Online]. Available: https://ansyshelp.ansys.com/public/account/secured?returnurl=/Views/Secured/corp/v251/en/flu_ug/pt01.html.

[5] *Prediction of Lift*. [Online]. Available: https://web.mit.edu/16.unified/www/SPRING/fluids/Lecture_Notes/f18.pdf.

[6] L. M. Thomson, *Theoretical Aerodynamics*. Dover Publications, 1958.

[7] S. K. S. W. Carla N. D. Sheridan Dahlia D. V. Pham, “Evaluation of vspaero analysis capabilities for conceptual design of aircraft with propeller-blown wings,” [Online]. Available: https://ntrs.nasa.gov/api/citations/20210017397/downloads/SheridanPham2021%200805.pdf.

[8] M. S. G. Samuel and P. Rajendran, “Cfd validation of naca 2412 airfoil,” Apr. 2019. DOI: 10.13140/RG.2.2.16245.42723.

[9] F. R. Menter, “Two-equation eddy-viscosity turbulence models for engineering applications,” *AIAA Journal*, vol. 32, no. 8, pp. 1598–1605, 1994. DOI: 10.2514/3.12149. [Online]. Available: https://doi.org/10.2514/3.12149.

[10] C. B. Courtin and R. J. Hansman, “An assessment of electric stol aircraft,” M.S. thesis, Massachusetts Institute of Technology, 2019. [Online]. Available: https://hdl.handle.net/1721.1/122042.

[11] D. A. Spence, “The lift coefficient of a thin, jet-flapped wing,” [Online]. Available: https://royalsocietypublishing.org/doi/10.1098/rspa.1956.0203.

[12] A. O. Demuren, “Modeling jets in cross flow,” [Online]. Available: https://ntrs.nasa.gov/api/citations/19950005517/downloads/19950005517.pdf.